Sensors and Materials, Vol. 37, No. 4 (2025) 1773–1783
MYU Tokyo

S & M 4017

Dual-window Coupled Dual-mode Substrate Integrated Waveguide Filter with Multiple Transmission Zeros for Point-to-point Communication of Automated Guided Vehicle

Xiaogang Li,[1] Yanggao Xu,[1] Tianwen Guo,[1*] Wencai Li,[1]
Hongli Deng,[1] Yawen He,[2] Haitao Xing,[2] and Zhonghua Ma[2**]

[1]Longyan Tobacco Industry Co., Ltd., Longyan, Fujian 364000, China
[2]School of Marine Information Engineering, Jimei University, Xiamen, Fujian 361021, China

(Received January 17, 2025; accepted April 17, 2025)

Keywords: bandpass filter, dual mode, substrate integrated waveguide (SIW), transmission zeros, insertion loss, relative bandwidth

A dual-window coupled dual-mode cavity substrate integrated waveguide (SIW) filter is proposed for automated guided vehicle (AGV) point-to-point communication, where two pairs of transmission zeros (TZs) are achieved on both sides of the passband. The dual-mode cavity is realized by inwardly folding one corner of the SIW cavity, with a perturbation via placed at the diagonal position. The TE_{102} and TE_{201} modes are mainly utilized by the dual-mode SIW filter. Coupling between the two cavities is achieved through openings in the via wall, and the position of the first resonance point in the passband can be adjusted by changing the width of the coupling window. The second and third resonance points can be altered by adjusting the distance of the perturbation via from the sidewall. The positions of the TZs on both sides of the passband can be modified by adjusting the offset distance of the input/output ports from the centerline and the length of the folded angle from the sidewall. Magnetic coupling between the two dual-mode SIW cavities is achieved through a dual-window structure, resulting in two pairs of TZs on either side of the passband, thereby improving frequency selectivity. A fourth-order SIW filter with two pairs of TZs has been simulated, fabricated, and measured. The measured frequency response shows good agreement with the simulated results, with a center frequency f_0 of 29.3 GHz, a minimum insertion loss of 1.4 dB, and a return loss better than 11 dB. Four TZs are observed at 24.68, 27, 31.06, and 35.12 GHz, with suppression better than 20 dB. The filter can be applied in wireless electromagnetic systems, such as microwave sensor systems, 6G mm-wave communication, or point-to-point communication for AGV vehicles.

1. Introduction

In modern communication systems, higher demands have been placed on the out-of-band suppression of bandpass filters to mitigate out-of-band interference. Quasi-elliptic filters have attracted significant attention in modern signal processing and communication systems owing to

*Corresponding author: e-mail: gtw22338@fjtic.cn
**Corresponding author: e-mail: mzhxm@jmu.edu.cn
https://doi.org/10.18494/SAM5549

ISSN 0914-4935
https://myukk.org/

their excellent performance in frequency selectivity, passband flatness, and stopband attenuation.[1–4] Moreover, substrate-integrated waveguide (SIW) technology has gained increasing popularity in recent years for its low cost, lightweight design, and good integration with planar microwave circuits.[5–9] To address the complex and variable communication environment and effectively filter out interference signals, various SIW filters with different structures and characteristics have been proposed by researchers over the past two decades.[10–16]

As spectrum resources become increasingly scarce and signal quality requirements rise, there is an urgent need to develop filters with high out-of-band suppression to ensure signal clarity and stability in wireless communication, radar, and satellite communication systems. One common approach is the use of slotline perturbations. By introducing slotlines into the filter structure, the electromagnetic wave propagation characteristics can be effectively adjusted, and the frequency response can be optimized to achieve the desired transmission zeros (TZs).[17,18] However, excessive slotline perturbations may weaken the structural stability of the filter and lead to additional insertion loss in high-frequency applications. Another common method is the incorporation of resonators, such as microstrip or ring resonators. By adjusting the size, shape, and spacing of the resonators, the position of the TZs can be precisely controlled to optimize filter performance.[19,20] However, the resonator design is often complex and requires precise parameter control to ensure the formation of the desired TZs. Increasing the number of resonators may result in larger sizes, affecting overall integration. Multilayer structure design offers a flexible solution for introducing TZs by increasing the mode freedom through interlayer coupling, thereby enhancing overall performance.[21–23] However, multilayer designs also introduce manufacturing complexity and higher costs, and they may face challenges in terms of fabrication difficulty and assembly precision in practical applications.

In this paper, a method is proposed to cascade two dual-mode SIW filters through dual-window coupling to achieve two pairs of TZs on both sides of the passband. The design does not require additional structures, optimizing the simplicity and efficiency of the design, making the process of achieving TZs more effective. By placing a perturbation via at the lower-right diagonal of the SIW cavity and folding the metal via on the upper-left diagonal, the resonance frequency of the TE_{102} mode is separated from that of the TE_{201} mode, forming a dual-mode resonant cavity. Additionally, by adjusting the offset distance of the ports from the centerline, the positions of the TZs can be flexibly altered. Ultimately, a fourth-order filter is formed by cascading two dual-mode cavities through dual coupling windows, successfully achieving two pairs of TZs and significantly improving frequency selectivity. To verify the proposed method, a filter prototype operating at 29.3 GHz was designed, with a relative bandwidth of 9.38% and stopband suppression better than 20 dB. Four TZs were obtained, and the measured frequency response agrees well with the simulated results. As an important part of microwave sensor systems, the proposed dual-mode SIW bandpass filter with two pairs of out-of-band TZs can be readily implemented and is suitable for various applications, such as mm-wave communication and point-to-point communication in automated guided vehicles.

2. Design and Analysis of Dual-mode SIW Filter

2.1 Rectangular SIW cavity

Figure 1 shows a rectangular SIW cavity with a side length of W. The sidewalls of the cavity are formed by a series of metallic vias with a diameter of d_1 and a spacing of p. Only the TE_{m0n} mode is supported within the cavity, and the resonant frequency of the TE_{m0n} mode in the proposed SIW cavity can be calculated as[24]

$$f_{TE_{m0n}} = \frac{c}{2\sqrt{\mu_r \varepsilon_r}} \sqrt{\left(\frac{m}{W}\right)^2 + \left(\frac{n}{W}\right)^2} . \quad (1)$$

Here, c is the speed of light in vacuum, μ_r and ε_r are the relative magnetic permeability and relative permittivity, respectively, and m and n are the mode indices along the two directions of the cavity. A Rogers RT/period 5880 substrate is used in the SIW cavity design, with a thickness (h) of 0.508 mm, a relative dielectric constant (ε_r) of 2.2, and a loss tangent (tan δ) of 0.0009.

The proposed dual-mode filter utilizes the TE_{201} and TE_{102} modes of the rectangular SIW cavity. Figure 2 shows the variations in electric field vector for the TE_{201} and TE_{102} modes within the rectangular SIW cavity. It can be observed that TE_{201} and TE_{102} form the first pair of degenerate dual modes, with these two modes being orthogonal to each other.

High-Frequency Structure Simulator (HFSS) software simulations show that the resonant frequency of the fundamental mode TE_{101} is 18.83 GHz, which is significantly lower than those of the degenerate modes TE_{201} and TE_{102}. Therefore, the dual-mode filter can be designed using the degenerate modes TE_{201} and TE_{102} by separating the resonant frequency of the TE_{102} mode from that of the TE_{201} mode. To increase the resonant frequency of the TE_{102} mode, a perturbation via has been added to the lower-right diagonal of the rectangular SIW cavity and

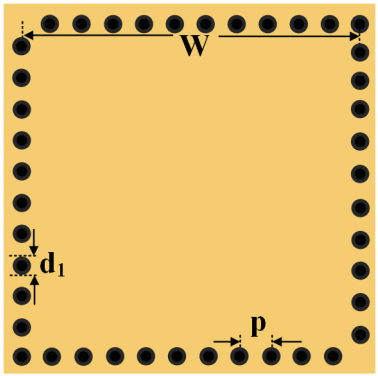

Fig. 1. (Color online) Top view of rectangular SIW cavity.

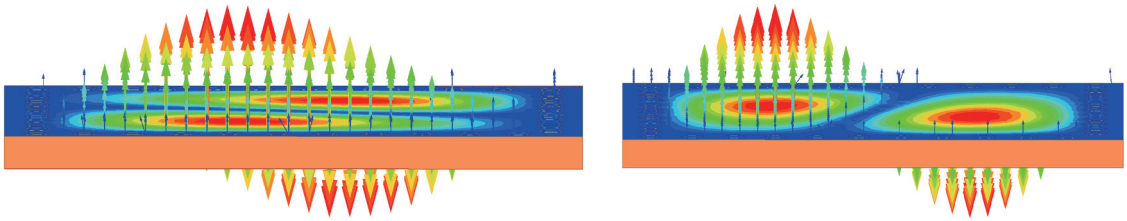

(a) (b)

Fig. 2. (Color online) Variations in electric field vector for degenerate modes in rectangular SIW cavity: (a) TE_{201} mode and (b) TE_{102} mode.

the metallic via on the upper-left diagonal sidewall has been inwardly folded, as shown in Fig. 3. Here, t represents the distance from the folded metallic via to the sidewall, and *Offset* represents the distance from the perturbation via to the sidewall metallic via. The diameter of all the metallic vias on the SIW sidewalls is $d_1 = 0.4$ mm, the diameter of the perturbation via is $d_2 = 0.5$ mm, and the spacing between two adjacent vias is $p = 0.75$ mm.

The dual-mode structure results in a slight change in resonant frequency between the TE_{101} and TE_{201} modes, while a significant increase is observed for the TE_{102} mode. HFSS software simulations provide the resonant frequencies of the TE_{101}, TE_{201}, and TE_{102} modes of the dual-mode SIW cavity as 18.83, 29.20, and 30.49 GHz, respectively. Compared with the resonant frequency of the empty cavity, that of the TE_{102} mode in the dual-mode cavity increases, while those of the TE_{101} and TE_{201} modes remain nearly unchanged.

2.2 Design of a fourth-order dual-mode filter

To improve the out-of-band roll-off rate, a dual-window coupling structure is introduced to enhance the out-of-band suppression performance of the filter. The geometric configuration and topological structure of the proposed dual-cavity dual-mode SIW filter are shown in Figs. 4(a) and 4(b), respectively. In the schematic diagram of the structure shown in Fig. 4(a), a fourth-order SIW filter is realized by cascading two identical dual-mode SIW cavities through dual-window coupling. The input and output ports of the dual-mode SIW filter are offset in opposite directions from the horizontal centerline (dashed white line) of the rectangular cavity, with an offset distance S from the centerline of the metallic via wall. The internal coupling between the two dual-mode SIW cavities is achieved through the opening in the via wall located on the horizontal centerline. Both cavities are excited by the TE_{201} and TE_{102} modes. The topological structure of the proposed fourth-order dual-mode SIW filter is illustrated in Fig. 4(b), with the gray shaded area representing the two modes of one cavity. Node N is a nonresonant node that provides an additional transmission path, introducing a TZ point on both sides of the filter passband through the energy superposition of different coupling paths, thereby enhancing the filter's selectivity and out-of-band suppression. When the amplitudes of the signals transmitted through the coupling paths S-N-L and S-1/2-3/4-L are equal but opposite in phase, a TZ point can be generated according to the principle of energy cancellation. Thus, this structure can produce two pairs of TZ points.

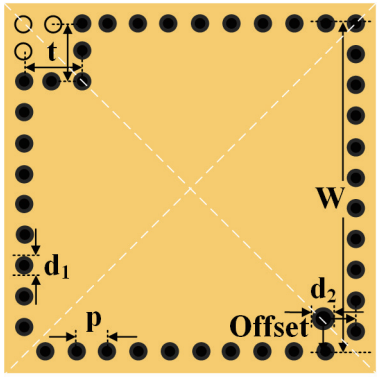

Fig. 3. (Color online) Structure of dual-mode SIW cavity.

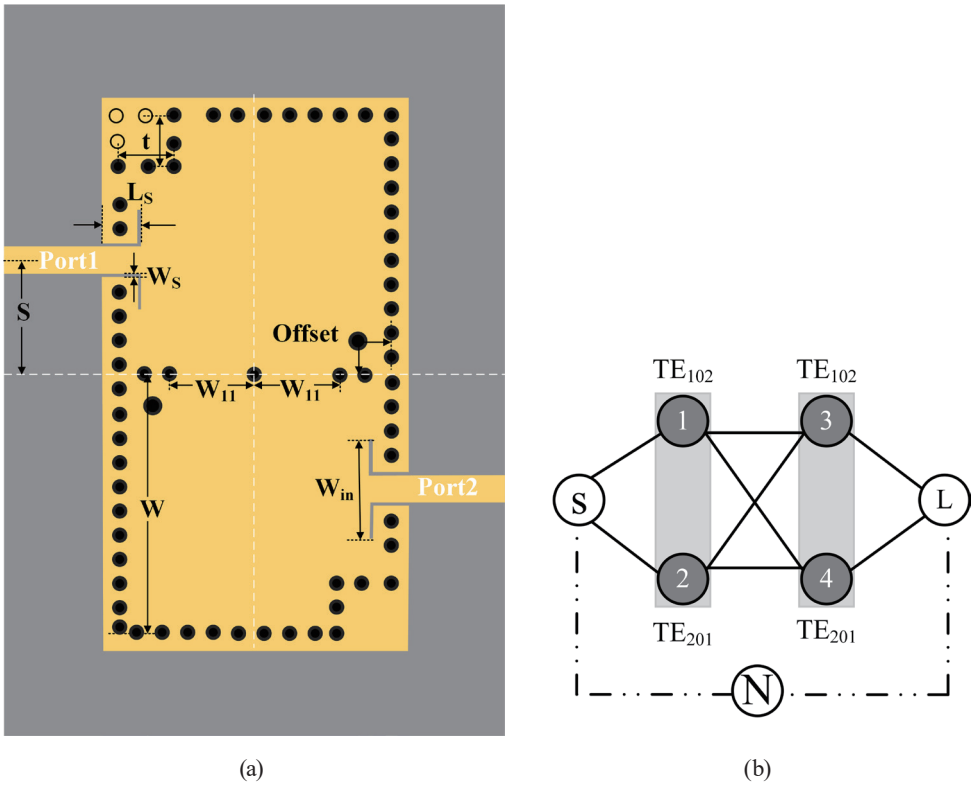

(a) (b)

Fig. 4. (Color online) (a) Geometric configuration and (b) topological structure of the fourth-order SIW filter with dual-window coupling.

To demonstrate complete control over the positions of the TZs, analyses of the offset distance S and the distance t from the corner to the sidewall are conducted. Figure 5 shows the transmission characteristic S_{21} curves for different S values. From Fig. 5, it can be observed that as S decreases, the TZ_2 on the left side of the passband shows minor changes and shifts slightly to higher frequencies, while the TZ_3 on the right side of the passband remains largely unchanged.

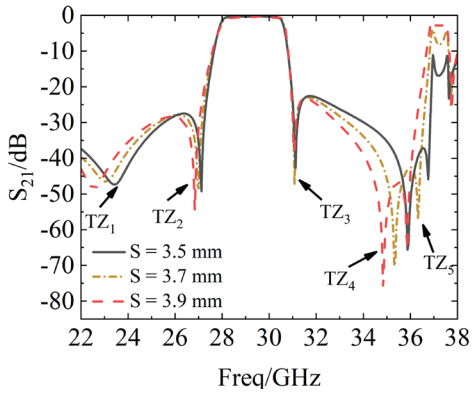

Fig. 5. (Color online) Effect of varying S on the positions of TZs in the SIW filter.

The low-frequency TZ_1 and the high-frequency TZ_4 and TZ_5 outside the passband exhibit significant changes, all shifting to higher frequencies, and a parasitic passband appears at 37 GHz outside the passband. Figure 6 shows the transmission characteristic S_{21} curves for different t values from the corner to the sidewall. From Fig. 6, it can be seen that as t increases, the TZ_2 on the left side of the passband remains mostly unchanged, while the TZ_3 on the right side of the passband shows considerable changes and shifts to higher frequencies. The low-frequency TZ_1 outside the passband remains mostly unchanged, whereas the high-frequency TZ_4 and TZ_5 show significant shifts to higher frequencies, with a parasitic passband appearing at 37 GHz outside the passband. Therefore, both S and t can be adjusted together to control the positions of the TZ points.

To demonstrate control over the positions of the resonance points, the parameters *Offset* and W_{11} are analyzed. Figure 7 shows the transmission characteristic S_{11} curves for different *Offset* values from the perturbing via to the sidewall. From Fig. 7, it can be observed that as *Offset* decreases, the second and third resonance points move closer to each other. When *Offset* is set to 1 mm, the reflection within the passband is minimized. Figure 8 shows the transmission characteristic S_{11} curves for different coupling window width W_{11} values. From Fig. 8, it can be seen that as W_{11} decreases, the first resonance point shifts to higher frequencies, while the other resonance points show minimal changes. Variations in *Offset* and W_{11} have little impact on the bandwidth but significantly affect the reflection characteristics within the passband. Therefore, *Offset* and W_{11} can be adjusted to control the position changes of the resonance points.

3. Results and Discussion

To verify the proposed method, a fourth-order single-layer dual-mode filter was designed using the TE_{201} and TE_{102} modes of the rectangular SIW cavity. This filter operates at a frequency of 29.3 GHz with a fractional bandwidth (FBW) of 9.38%. The designed filter has been fabricated, and its characteristics were measured using a vector network analyzer. Figure 9 shows the prototype of the designed filter, providing a visual representation of its layout.

The final dimensions are given as follows: W = 8 mm, W_{11} = 2.5 mm, S = 3.5 mm, L_S = 1.15 mm, W_S = 0.1 mm, W_{in} = 3.23 mm, *Offset* = 1 mm, and t = 1.6 mm. Figure 10 shows the

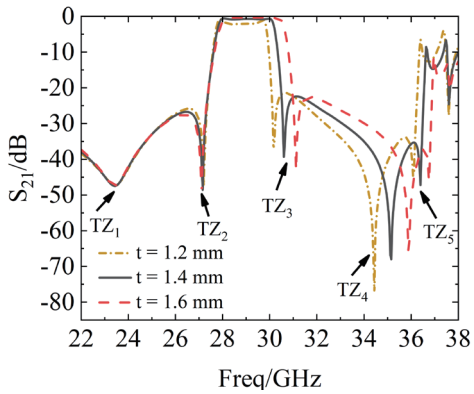

Fig. 6. (Color online) Effect of varying t on the positions of TZs in the SIW filter.

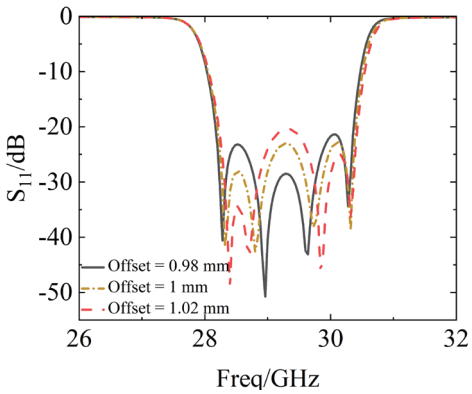

Fig. 7. (Color online) Effect of varying *Offset* on the positions of resonance points in the SIW filter.

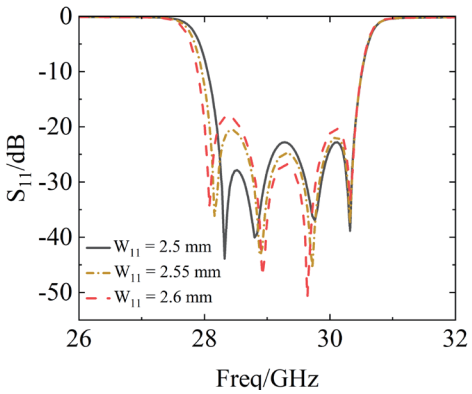

Fig. 8. (Color online) Effect of varying W_{11} on the positions of resonance points in the SIW filter.

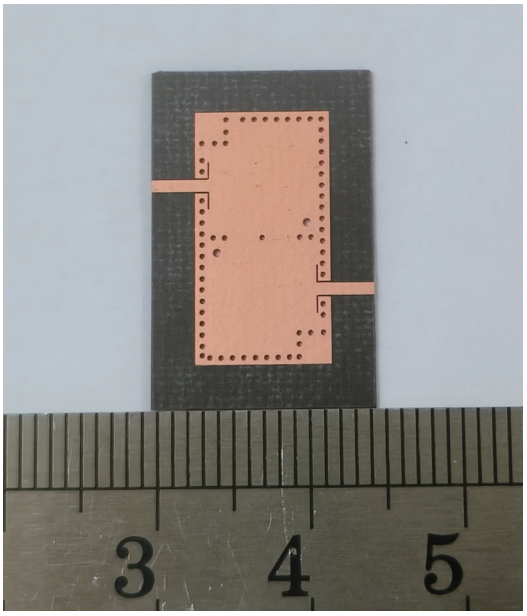

Fig. 9. (Color online) Photograph of fourth-order SIW filter with dual-window coupling.

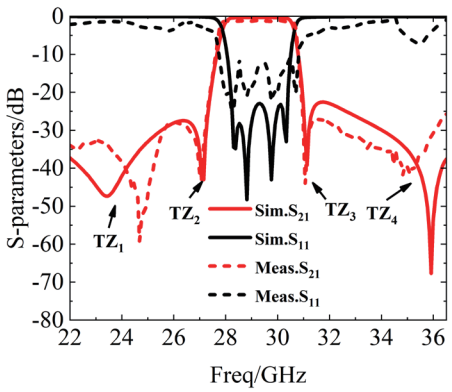

Fig. 10. (Color online) *S*-parameters of fourth-order SIW filter with dual-window coupling.

Table 1
Results of work presented in this paper and other reported works.

Ref.	f_0 (GHz)	FBW (%)	IL (dB)	NP	NZ	Layers	Size (λ_g^2)
25	10	4	1.98	4	2	1	1.98
26	12.48	3.74	1.34	4	2	1	2.78
27	10	3.5	2.04	5	2	1	3.77
28	15	4.3	2.6	6	2	1	3.5
29	9.99	10.9	0.87	4	2	1	1.89
30	9	2.1	2.8	3	2	2	0.46
This work	29.3	9.38	1.4	4	4	1	2.69

f_0: center frequency; FBW: fractional bandwidth; IL: insertion loss; NP: number of poles; NZ: number of TZs.

simulated and measured responses. The measured results are in good agreement with the simulated results. The simulated center frequency (f_0) is 29.3 GHz, with a FBW of 9.38%. The minimum insertion loss is 0.32 dB, and the return loss is better than 22.92 dB. Two TZs can be observed in the lower stopband at 23.44 and 27.11 GHz, and two TZs can also be seen in the upper stopband at 31.12 and 35.93 GHz, with suppression greater than 20 dB. The measured f_0 is 29.3 GHz, with a minimum insertion loss of 1.4 dB and a return loss better than 11 dB. Four TZs are obtained at 24.68, 27, 31.06, and 35.12 GHz, with suppression greater than 20 dB. The differences between the simulated and measured return losses in Fig. 10 are primarily attributed to dimensional errors during the manufacturing process, deviations during the soldering of the subminiature version A (SMA) connectors, and slight discrepancies between material properties and ideal design parameters. Additionally, uncertainties in the measurement environment and equipment precision may also affect the results.

Table 1 shows the proposed dual-window coupled fourth-order SIW filter with other reported designs. From the parameter data in Table 1, it can be seen that the SIW BPF proposed in this paper achieves a wider bandwidth, lower insertion loss, and more compact size in the high-frequency range. Note that the filters with the designs described in Refs. 25–28 operate at lower frequencies and have fewer TZs with relatively narrow bandwidths. Although a wider bandwidth and lower insertion loss were achieved by Zhu *et al.*,[29] it only has two TZs and is based on a microstrip pole-extracting resonator, resulting in a higher complexity of fabrication. Owing to a complex multilayer structure, the miniaturized size was achieved by Chu *et al.*[30] The size

comes at the cost of a narrower bandwidth and fewer poles. Therefore, the proposed single-layer design demonstrates significant advantages by combining a wider bandwidth, low insertion loss, and more TZs under high-frequency operation.

4. Conclusions

In the paper, a dual-window coupled dual-cavity dual-mode SIW filter is proposed. The filter can achieve two pairs of TZs, thereby enhancing frequency selectivity. The working principle of the proposed dual-mode bandpass filter is detailed. The filter is designed using the TE_{201} and TE_{102} modes of a rectangular SIW cavity. The designed fourth-order dual-mode SIW filter has been fabricated, and its characteristics have been tested, validating the proposed design method. The measured results are in good agreement with the simulated results. In microwave sensor systems, SIW bandpass filters are commonly used to fulfill system signal processing requirements. This technology is expected to be a competitive candidate for developing high-performance SIW filters in microwave communication systems.

Acknowledgments

This work was supported by the China Tobacco Fujian Industry Co., Ltd. 2023 External Technical Cooperation Project (FJZYHZJH2023018).

References

1 Q. Liu, D. F. Zhou, K. Gong, J. H. Wang, D. W. Zhang, and B. H. Ma: IEEE Trans. Circuits Syst. II Express Briefs **71** (2024) 1994. https://doi.org/10.1109/TCSII.2023.3335183
2 J. L. Olvera-Cervantes, A. Corona-Chavez, D. V. B. Murthy, and H. Lobato-Morals: IEICE Electron. Express **6** (2009) 1143. https://doi.org/10.1587/elex.6.1143
3 D. Liu and Y. Dong: IEEE Trans. Circuits Syst. II Express Briefs **69** (2022) 4248. https://doi.org/10.1109/TCSII.2022.3188528
4 Y. Song, G. H. Liu, and Z. Q. Cheng: IEICE Electron. Express **20** (2023) 18. https://doi.org/10.1587/elex.20.20230311
5 P. L. Chi, T. C. Yeh, and T. Yang: IEEE Access **12** (2024) 137870. https://doi.org/10.1109/ACCESS.2024.3464234
6 H. K. Chen, Y. Shao, Y. J. Zhang, C. H. Zhang, and Z. Z. Zhang: IEEE Trans. Antennas Propag. **68** (2020) 8162. https://doi.org/10.1109/TAP.2020.2996806
7 L. Y. Wang, H. W. Chen, W. L. Li, J. H. Zhang, L. B. Gao, X. Z. Cai, Z. Fang, Y. Li, Y. Zhu, and R. Zhang: IEEE Trans. Compon. Packag. Manuf. Technol. **13** (2023) 2008. https://doi.org/10.1109/TCPMT.2023.3333410
8 D. Deslandes and K. Wu: IEEE Trans. Microwave Theory Tech. **54** (2006) 2516. https://doi.org/10.1109/TMTT.2006.875807
9 X. L. Yang, X. W. Zhu, and D. Y. Huang: IEEE Microwave Wireless Tech. Lett. **34** (2024) 1178. https://doi.org/10.1109/LMWT.2024.3439733
10 D. Li, J. Wang, L. Shi, Y. Liu, K. Xu, Q. Chen, and N. Shinohara: IEEE Microwave Wireless Tech. Lett. **34** (2024) 482. https://doi.org/10.1109/LMWT.2024.3382592
11 P. Chu, W. Hong, M. G. Tuo, K. L. Zheng, W. W. Yang, F. Xu, and K. Wu: IEEE Trans. Microwave Theory Tech. **65** (2017) 824. https://doi.org/10.1109/TMTT.2016.2633346
12 Q. Liu, J. J. Wei, K. Gong, H. Qian, B. H. Ma, and D. W. Zhang: IEEE Trans. Circuits Syst. II Express Briefs **70** (2023) 4369. https://doi.org/10.1109/TCSII.2023.3285661
13 Q. Liu, N. An, Z. Y. He, D. W. Zhang, X. Wang, and D. F. Zhou: IET Microwaves Antennas Propag. **15** (2021) 1. https://doi.org/10.1049/mia2.12017
14 P. Chu, P. Zhu, J. G. Feng, L. Guo, L. Zhang, F. Zhu, L. L. Liu, G. Q. Luo, and K. Wu: IEEE Trans. Microwave Theory Tech. **71** (2023) 4003. https://doi.org/10.1109/TMTT.2023.3251567

15 Y. Zheng, H. Tian, and Y. Dong: Chin. J. Electron. **33** (2024) 456. https://doi.org/10.23919/cje.2023.00.057
16 C. Fan, X. Liu, N. Liu, and Z. Zhu: IEEE Trans. Microwave Theory Tech. **72** (2024) 5095. https://doi.org/10.1109/TMTT.2024.3370823
17 P. Chu, P. Zhu, J. G. Feng, L. Guo, L. Zhang, F. Zhu, L. L. Liu, G. Q. Luo, and K. Wu: IEEE Trans. Microwave Theory Tech. **71** (2023) 4003. https://doi.org/10.1109/TMTT.2023.3251567
18 X. Wang, N. Y. Zhong, H. Y. Li, J. Y. Chu, H. Yang, X. L. Yang, X. W. Zhu, and W. Wu: IEEE Trans. Circuits Syst. II Express Briefs **71** (2024) 3655. https://doi.org/10.1109/TCSII.2024.3369046
19 Y. Zhu and Y. Dong: IEEE Trans. Circuits Syst. II Express Briefs **69** (2022) 719. https://doi.org/10.1109/TCSII.2021.3111860
20 Y. Zhu, Y. Dong, J. Bornemann, L. Gu, and D. F. Mamedes: IEEE Trans. Microwave Theory Tech. **71** (2023) 2193. https://doi.org/10.1109/TMTT.2022.3225447
21 P. Chu, J. G. Feng, P. Zhu, L. Guo, L. Zhang, L. L. Liu, G. Q. Luo, K. Wu, and S. L. Pan: Chin. J. Electron. **33** (2024) 436. https://doi.org/10.1109/TCSII.2023.3335183 10.23919/cje.2023.00.027
22 Q. Liu, L.-S. Wu, D.-F. Zhou, K. Gong, and D.-W. Zhang: IEEE Trans. Circuits Syst. I Regul. Pap. **71** (2024) 3098. https://doi.org/10.1109/TCSII.2023.3335183
23 G. Zhang, X. Zhou, J. H. Hu, K. W. Tam, D. S. Li, Z. W. Zhang, T. Y. Ma, and J. Q. Yang: IEEE Trans. Compon. Packag. Manuf. Technol. **14** (2024) 114. https://doi.org/10.1109/TCPMT.2023.3330170
24 Q. Liu, D. W. Zhang, M. Tang, H. L. Deng, and D. F. Zhou: IEEE Trans. Microwave Theory Tech. **69** (2021) 101. https://doi.org/10.1109/TMTT.2020.3037497
25 D. Li, W. Luo, X. Q. Chen, J. X. Wang, C. Yang, K. D. Xu, and Q. Chen: IEEE Trans. Circuits Syst. II Express Briefs **71** (2024) 3338. https://doi.org/10.1109/TCSII.2024.3364816
26 Q. Liu, D. F. Zhou, Y. Zhang, D. W. Zhang, and D. L. Lv: IEEE Trans. Microwave Theory Tech. **67** (2019) 1014. https://doi.org/10.1109/TMTT.2018.2889450
27 F. Zhu, G. Q. Luo, B. You, X. H. Zhang, and K. Wu: IEEE Trans. Microwave Theory Tech. **69** (2021) 3048. https://doi.org/10.1109/TMTT.2021.3074617
28 P. Chu, L. Guo, L. Zhang, F. Xu, W. Hong, and K. Wu: IEEE Trans. Microwave Theory Tech. **68** (2020) 964. https://doi.org/10.1109/TMTT.2019.2947894
29 Y. Zhu, Y. Dong, J. Bornemann, L. Gu, and D. F. Mamedes: IEEE Trans. Circuits Syst. II Express Briefs **70** (2023) 1856. https://doi.org/10.1109/TCSII.2022.3231577
30 P. Chu, J. G. Feng, L. Guo, L. Zhang, W. W. Yang, L. L. Liu, F. Xu, and K. Wu: IEEE Trans. Circuits Syst. II Express Briefs **70** (2023) 2744. https://doi.org/10.1109/TCSII.2023.3248095

About the Authors

Li Xiaogang received his bachelor's degree from Fuzhou University in China in 1995. From 1995 to 2009, he worked as an engineer at Longyan Tobacco Industry Co., Ltd. in China, and since 2010, he has been a senior engineer at the factory. His research interests are in automatic control, logistics technology, and big data. (lxg22089@fjtic.cn)

Xu Yanggao received his bachelor's degree from Fuzhou University in China in 1998. Since 1998, he has been working in the field of logistics automation and informatization at Longyan Tobacco Industry Co., Ltd. in China. His research interests are in industrial automation, IoT, and information technology. (xyg22210@fjtic.cn)

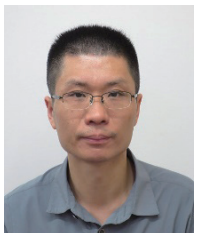

Guo Tianwen received his bachelor's degree from Chongqing University in China in 2002. In 2003 and 2017, he worked as an engineer at Longyan Cigarette Factory in China, and since 2018, he has been serving as a senior engineer at the factory. His research interests are in IoT, big data, and information technology. (gtw22338@fjtic.cn)

Li Wencan received his bachelor's degree from Hebei University of Engineering in China in 2003. From 2004 to 2022, he served as an engineer at Longyan Cigarette Factory in China and has been promoted to senior engineer at the factory since 2023. His research focuses on automation control, intelligent logistics technology, machine vision, and information technology. (lwc22355@fjtic.cn)

Deng Hongli received his bachelor's degree in engineering from Fuzhou University in China in 2019. From 2020 to 2024, he worked as an assistant engineer in China Longyan Cigarette Factory. Since 2024, he has been working as an engineer in the factory. His research interests are in artificial intelligence, generative modeling languages, and emerging information technologies. (dhl23399@fjtic.cn)

He Yawen received her bachelor's degree in communication engineering from Wuyi University, Nanping, China, in 2023. She is currently working toward a postgraduate degree in information and communication engineering at Jimei University, Xiamen, China. Her research interest is in RF microwave millimeter wave circuit design. (yw_he@jmu.edu.cn)

Xing Haitao received his master's degree in communication and information engineering from Ningbo University in 2010. At present, his main research interests are in embedded systems, artificial intelligence, and IoT. (xht2005@jmu.edu.cn)

Ma Zhonghua received his Ph.D. degree in microelectronics from Lanzhou University, Lanzhou, in 2018. His present research interests include antenna techniques, RF and microwave circuit design, and IoT. (mzhxm@jmu.edu.cn)